Inorganic Chemistry

Article

pubs.acs.org/IC

New Vanadium Selenites: Centrosymmetric $Ca_2(VO_2)_2(SeO_3)_3(H_2O)_2$, $Sr_2(VO_2)_2(SeO_3)_3$, and $Ba(V_2O_5)(SeO_3)$, and Noncentrosymmetric and Polar $A_4(VO_2)_2(SeO_3)_4(Se_2O_5)$ (A = Sr^{2+} or Pb^{2+})

Jeongho Yeon, Sang-Hwan Kim, Sau Doan Nguyen, Hana Lee, and P. Shiv Halasyamani*

Department of Chemistry, University of Houston, 136 Fleming Building, Houston, Texas 77204-5003, United States

Supporting Information

ABSTRACT: Five new vanadium selenites, $Ca_2(VO_2)_2(SeO_3)_3(H_2O)_2$, $Sr_2(VO_2)_2(SeO_3)_3$, $Ba(V_2O_5)(SeO_3)$, $Sr_4(VO_2)_2(SeO_3)_4(Se_2O_5)$, and $Pb_4(VO_2)_2(SeO_3)_4(Se_2O_5)$, have been synthesized and characterized. Their crystal structures were determined by single crystal X-ray diffraction. The compounds exhibit one- or two-dimensional structures consisting of corner- and edge-shared VO_4, VO_5, VO_6, and SeO_3 polyhedra. Of the reported materials, $A_4(VO_2)_2(SeO_3)_4(Se_2O_5)$ (A = Sr^{2+} or Pb^{2+}) are noncentrosymmetric (NCS) and polar. Powder second-harmonic generation (SHG) measurements revealed SHG efficiencies of approximately 130 and 150 × α−SiO_2 for $Sr_4(VO_2)_2(SeO_3)_4(Se_2O_5)$ and $Pb_4(VO_2)_2(SeO_3)_4(Se_2O_5)$, respectively. Piezoelectric charge constants of 43 and 53 pm/V, and pyroelectric coefficients of −27 and −42 $\mu C/m^2 \cdot K$ at 70 °C were obtained for $Sr_4(VO_2)_2(SeO_3)_4(Se_2O_5)$ and $Pb_4(VO_2)_2(SeO_3)_4(Se_2O_5)$, respectively. Frequency dependent polarization measurements confirmed that the materials are not ferroelectric, that is, the observed polarization cannot be reversed. In addition, the lone-pair on the Se^{4+} cation may be considered as stereo-active consistent with calculations. For all of the reported materials, infrared, UV−vis, thermogravimetric, and differential thermal analysis measurements were performed. Crystal data: $Ca_2(VO_2)_2(SeO_3)_3(H_2O)_2$, orthorhombic, space group *Pnma* (No. 62), a = 7.827(4) Å, b = 16.764(5) Å, c = 9.679(5) Å, V = 1270.1(9) Å^3, and Z = 4; $Sr_2(VO_2)_2(SeO_3)_3$, monoclinic, space group $P2_1/c$ (No. 12), a = 14.739(13) Å, b = 9.788(8) Å, c = 8.440(7) Å, β = 96.881(11)°, V = 1208.8(18) Å^3, and Z = 4; $Ba(V_2O_5)(SeO_3)$, orthorhombic, space group *Pnma* (No. 62), a = 13.9287(7) Å, b = 5.3787(3) Å, c = 8.9853(5) Å, V = 673.16(6) Å^3, and Z = 4; $Sr_4(VO_2)_2(SeO_3)_4(Se_2O_5)$, orthorhombic, space group *Fdd*2 (No. 43), a = 25.161(3) Å, b = 12.1579(15) Å, c = 12.8592(16) Å, V = 3933.7(8) Å^3, and Z = 8; $Pb_4(VO_2)_2(SeO_3)_4(Se_2O_5)$, orthorhombic, space group *Fdd*2 (No. 43), a = 25.029(2) Å, b = 12.2147(10) Å, c = 13.0154(10) Å, V = 3979.1(6) Å^3, and Z = 8.

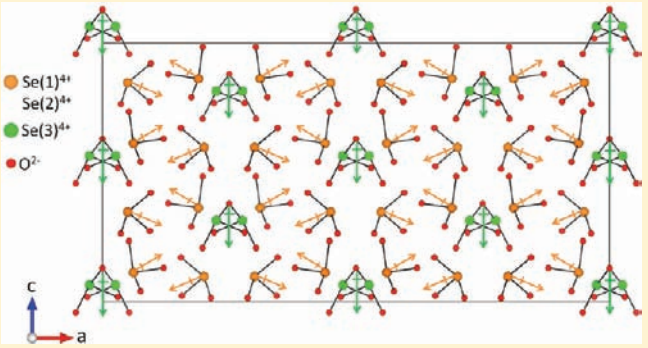

INTRODUCTION

Asymmetric coordination environments in noncentrosymmetric (NCS) polar materials are of significant interest attributable to their potential impact on the observed macroscopic polarity. This macroscopic polarity is required for technologically important properties such as ferroelectricity and pyroelectricity.[1−3] Other "acentric" properties, that is, second-harmonic generation (SHG) and piezoelectricity, require NCS structures but not necessarily NCS *polar* structures.[4−6] Crystallographically, a material is considered polar if it is found in one of 10 polar crystal classes (1, 2, 3, 4, 6, m, mm2, 3 m, 4 mm, or 6 mm).[7] A number of strategies have been published on the design and synthesis of new polar materials.[8−34] We have focused on using cations susceptible to second-order Jahn−Teller (SOJT) distortions,[35−41] that is, octahedrally coordinated d^0 cations (Ti^{4+}, Nb^{5+}, W^{6+}, etc.) and cations with a stereo-active lone-pair (Se^{4+}, Te^{4+}, I^{5+}, etc.).[6,19,30,33,42−51] With both families, the cations are in asymmetric and locally polar coordination environments. When these coordination environments are aligned in the structure, that is, "constructively add", a macroscopically polar material is created.

With respect to oxides that contain V^{5+} and Se^{4+}, a number of materials have been reported. These include $(VO)_2(SeO_3)_3$,[52] $(V_2O_3)(SeO_3)_2$,[53] $(VO)(SeO_3)_4(OH)(H_2O)_3$,[54] $Cd(VO_2)_4(SeO_3)_3(H_2O)$,[55] $K(VO)_2(SeO_3)$,[56] $A(VO_2)(SeO_3)$ (A = Rb^+, Cs^+, Tl^+, and Ag^+),[45,57,58] $A(VO_2)_3(SeO_3)_2$ (A = K^+, Rb^+, Cs^+, Tl^+, and NH_4^+),[47,57,59] $Ba(VO_2)(SeO_3)_2(HSeO_3)$,[59] $Ba_{2.5}(VO_2)_3(SeO_3)_4(H_2O)$,[60] $Pb_2(V_2O_5)(SeO_3)_2$,[18] and $Ba_3(VO_2)_2(SeO_3)_4$.[20] Of these materials, only $A(VO_2)(SeO_3)$ (A = Rb^+, Cs^+, and Tl^+),[45,57,58] $A(VO_2)_3(SeO_3)_2$ (A = K^+, Rb^+, Cs^+, Tl^+, and NH_4^+)[47,57,59] are NCS and polar. We have synthesized five new vanadium selenites, $Ca_2(VO_2)_2(SeO_3)_3(H_2O)_2$, $Sr_2(VO_2)_2(SeO_3)_3$, $Ba(V_2O_3)(SeO_3)$, $Sr_4(VO_2)_2(SeO_3)_4(Se_2O_5)$, and $Pb_4(VO_2)_2(SeO_3)_4(Se_2O_5)$. Of these, $Sr_4(VO_2)_2(SeO_3)_4(Se_2O_5)$ and $Pb_4(VO_2)_2(SeO_3)_4(Se_2O_5)$ are NCS and

Received: October 3, 2011
Published: December 6, 2011

   dx.doi.org/10.1021/ic2021403 | *Inorg. Chem.* 2012, 51, 609−619

Table 1. Crystallographic Data for $Ca_2(VO_2)_2(SeO_3)_3(H_2O)_2$, $Sr_2(VO_2)_2(SeO_3)_3$, $Ba(V_2O_5)(SeO_3)$, $Sr_4(VO_2)_2(SeO_3)_4(Se_2O_5)$, and $Pb_4(VO_2)_2(SeO_3)_4(Se_2O_5)$

formula	$Ca_2(VO_2)_2(SeO_3)_3(H_2O)_2$	$Sr_2(VO_2)_2(SeO_3)_3$	$Ba(V_2O_5)(SeO_3)$	$Sr_4(VO_2)_2(SeO_3)_4(Se_2O_5)$	$Pb_4(VO_2)_2(SeO_3)_4(Se_2O_5)$
fw	658.92	722	446.18	1262.12	1740.4
crystal system	orthorhombic	monoclinic	orthorhombic	orthorhombic	orthorhombic
space group	*Pnma* (No. 62)	$P\,2_1/c$ (No. 14)	*Pnma* (No. 62)	*Fdd*2 (No. 43)	*Fdd*2 (No. 43)
a (Å)	7.827(4)	14.739(13)	13.9287(7)	25.161(3)	25.029(2)
b (Å)	16.764(5)	9.788(8)	5.3787(3)	12.1579(15)	12.2147(10)
c (Å)	9.679(5)	8.440(7)	8.9853(5)	12.8592(16)	13.0154(10)
α (deg)	90	90	90	90	90
β (deg)	90	96.881(11)	90	90	90
γ (deg)	90	90	90	90	90
V (Å^3)	1270.1(9)	1208.8(18)	673.16(6)	3933.7(8)	3979.1(6)
Z	4	4	4	8	8
GOF (F^2)	0.936	1.085	1.045	1.088	1.019
Flack parameter				−0.001(9)	0.001(7)
$R(F)^a$	0.0283	0.0268	0.0170	0.0220	0.0279
$R_w(F_o^2)^b$	0.0641	0.0690	0.0404	0.0580	0.0679

$^aR(F) = \sum||F_o| - |F_c||/\sum|F_o|$. $^bR_w(F_o^2) = [\sum w(F_o^2 - F_c^2)^2/\sum w(F_o^2)^2]^{1/2}$.

polar. In this paper we report on the synthesis, structures, characterization, and structure−property relationships in five new vanadium selenites. In addition, for $Sr_4(VO_2)_2(SeO_3)_4(Se_2O_5)$ and $Pb_4(VO_2)_2(SeO_3)_4(Se_2O_5)$ we investigate their functional properties, specifically SHG, piezoelectricity, and polarization.

EXPERIMENTAL SECTION

Reagents. $Ca(OH)_2$ (Aldrich, 96+%), $Sr(OH)_2{\cdot}8H_2O$ (Aldrich, 95%), $Ba(OH)_2{\cdot}8H_2O$ (Fisher, 98.6%), $BaCO_3$ (Aldrich, 99+%), $SrCO_3$ (Aldrich, 99.9+%), PbO (Aldrich, 99.9+%), V_2O_5 (Aldrich, 99+%), SeO_2 (Alfa Aesar, 99.8%) were used as received.

Syntheses. Single crystals of the reported materials were grown by using hydrothermal techniques. 0.0983 g (1.33 mmol) of $Ca(OH)_2$, 0.0483 g (0.266 mmol) of V_2O_5, and 0.353 g (3.18 mmol) of SeO_2 for $Ca_2(VO_2)_2(SeO_3)_3(H_2O)_2$, 0.257 g (0.965 mmol) of $Sr(OH)_2{\cdot}8H_2O$, 0.0293 g (0.161 mmol) of V_2O_5, and 0.214 g (1.93 mmol) of SeO_2 for $Sr_2(VO_2)_2(SeO_3)_3$, 0.219 g (0.695 mmol) of $Ba(OH)_2{\cdot}8H_2O$, 0.126 g (0.695 mmol) of V_2O_5, and 0.154 g (1.39 mmol) of SeO_2 for $Ba(V_2O_5)(SeO_3)$, and 0.225 g (0.157 g) (0.845 mmol (0.702 mmol)) of $Sr(OH)_2{\cdot}8H_2O$ (PbO), 0.0256 g (0.0319 g) (0.141 mmol (0.175 mmol)) of V_2O_5, and 0.250 g (0.311 g) (2.25 mmol (2.81 mmol) of SeO_2 for $Sr(Pb)_4(VO_2)_2(SeO_3)_4(Se_2O_5)$, respectively, were combined with 5 mL of H_2O. The respective solutions were placed in 23 mL Teflon-lined autoclaves. The autoclaves were closed, gradually heated to 230 °C, held for 4 days, and cooled slowly to room temperature (RT) at a rate of 6 °C h^{-1}. The mother liquor was decanted from the products, which were recovered by filtration and washed with distilled water and acetone. For $Ca_2(VO_2)_2(SeO_3)_3(H_2O)_2$, pale yellow crystals, the only product from the reaction, was obtained in ∼90% yield based on V_2O_5. For $Sr_2(VO_2)_2(SeO_3)_3$ and $Sr_4(VO_2)_2(SeO_3)_4(Se_2O_5)$, pale yellow crystals were recovered in ∼70% yield based on V_2O_5. A $SrSeO_4$ impurity was also observed, but was removed through sonication of the products in water. With $Ba(V_2O_5)(SeO_3)$ and $Pb_4(VO_2)_2(SeO_3)_4(Se_2O_5)$, brown and pale yellow crystals were obtained in ∼20% yields based on V_2O_5 respectively. Impurity phases of $Ba_{2.5}(VO_2)_3(SeO_3)_4(H_2O)$[60] and $Pb_2(V_2O_5)(SeO_3)_2$[18] were also observed in $Ba(V_2O_5)(SeO_3)$ and $Pb_4(VO_2)_2(SeO_3)_4(Se_2O_5)$, respectively.

Bulk $Ba(V_2O_5)(SeO_3)$, $Sr_4(VO_2)_2(SeO_3)_4(Se_2O_5)$, and $Pb_4(VO_2)_2(SeO_3)_4(Se_2O_5)$ were prepared by conventional solid-state methods. A stoichiometric mixture of $BaCO_3$ (0.805 g, 4.08 mmol), V_2O_5 (0.742 g, 4.08 mmol), and SeO_2 (0.453 g, 4.08 mmol) for $Ba(V_2O_5)(SeO_3)$, and mixtures of $SrCO_3$ (PbO)(1.18 g, 8.00 mmol)(1.79 g, 8.00 mmol), V_2O_5 (0.364 g, 2.00 mmol), and SeO_2 (1.33 g, 12.0 mmol) for $Sr_4(VO_2)_2(SeO_3)_4(Se_2O_5)(Pb_4(VO_2)_2(SeO_3)_4(Se_2O_5))$, respectively, were thoroughly ground, pressed into a pellet, and introduced into separate pyrex tubes that were subsequently evacuated under vacuum and sealed to prevent vaporization of SeO_2. The tubes were heated to 310 °C (24 h), 350 and 270 °C (48 h) for $Ba(V_2O_5)(SeO_3)$ and $Sr(Pb)_4(VO_2)_2(SeO_3)_4(Se_2O_5)$, respectively, and then cooled slowly to RT. The purity of samples was confirmed by powder X-ray diffraction and is in good agreement with the calculated diffraction pattern from single crystal structures.

Single Crystal X-ray Diffraction. Crystals of $Ca_2(VO_2)_2(SeO_3)_3(H_2O)_2$ (0.08 × 0.01 × 0.01 mm), $Sr_2(VO_2)_2(SeO_3)_3$ (0.05 × 0.04 × 0.01 mm), $Ba(V_2O_5)(SeO_3)$ (0.04 × 0.02 × 0.01 mm), $Sr_4(VO_2)_2(SeO_3)_4(Se_2O_5)$ (0.10 × 0.08 × 0.08 mm), and $Pb_4(VO_2)_2(SeO_3)_4(Se_2O_5)$ (0.05 × 0.02 × 0.01 mm) were used for single crystal data collection. Data were collected using a Siemens SMART diffractometer equipped with a 1K CCD area detector using graphite-monochromated Mo Kα radiation. A hemisphere of data was collected using a narrow-frame method with scan widths of 0.30° in ω and an exposure time of 35−70 s per frame for the reported materials. The data were integrated using the Siemens SAINT program,[61] with the intensities corrected for Lorentz, polarization, air absorption, and absorption attributable to the variation in the path length through the detector faceplate. ψ−scans for the reported materials were used for the absorption correction on the hemisphere of data. All of the data were solved by direct methods using SHELXS−97 and refined using SHELXL−97.[62,63] All of the atoms were refined with anisotropic thermal parameters and converged for $I > 2\sigma(I)$. All calculations were performed using the WinGX-98 crystallographic software package.[64] Crystallographic data and selected bond lengths are given in Tables 1, 2, and 3.

Powder X-ray Diffraction. Powder XRD data were collected using a PANalytical X'Pert PRO diffractometer with Cu Kα radiation. The 2θ range was 5−60°, with a continuous scan manner. The powder XRD patterns for the reported materials are in excellent agreement with the calculated XRD patterns from the single crystal models (see Supporting Information, Figure S1).

Infrared Spectroscopy. IR spectra were recorded on a Matterson FTIR 5000 spectrometer in the 400−4000 cm^{-1} range (see Supporting Information, Figure S2).

UV−vis Diffuse Reflectance Spectroscopy. UV−vis reflectance data were collected on a Varian Cary 500 Scan UV−vis−NIR spectrophotometer over the spectral range 200−1500 nm at RT. Poly(tetrafluoroethylene) was used as a reference material. Reflectance spectra were converted to absorbance using the Kubelka−Munk function[65] (see Supporting Information, Figure S3).

Thermal Analyses. Thermogravimetric analysis (TGA) and differential thermal analysis (DTA) were carried out on EXSTAR

dx.doi.org/10.1021/ic2021403 | Inorg. Chem. 2012, 51, 609−619

Table 2. Selected Bond Distances (Å) for $Ca_2(VO_2)_2(SeO_3)_3(H_2O)_2$, $Sr_2(VO_2)_2(SeO_3)_3$, and $Ba(V_2O_5)(SeO_3)$

$Ca_2(VO_2)_2(SeO_3)_3(H_2O)_2$		$Sr_2(VO_2)_2(SeO_3)_3$		$Ba(V_2O_5)(SeO_3)$	
V(1)−O(1)	1.597(3)	V(1)−O(1)	1.612(3)	V(1)−O(1)	1.588(3)
V(1)−O(2)	1.677(3)	V(1)−O(2)	1.659(3)	V(1)−O(2)	1.835(2)
V(1)−O(2)	2.248(3)	V(1)−O(3)	1.958(3)	V(1)−O(2)	1.835(2)
V(1)−O(3)	1.953(3)	V(1)−O(4)	1.984(3)	V(1)−O(3)	2.022(2)
V(1)−O(4)	1.976(3)	V(1)−O(5)	2.005(3)	V(1)−O(3)	2.022(2)
V(1)−O(5)	2.232(3)			V(1)−O(4)	2.278(3)
		V(2)−O(6)	1.612(3)		
Se(1)−O(3)	1.718(3)	V(2)−O(7)	1.673(3)	V(2)−O(5)	1.626(3)
Se(1)−O(4)	1.748(3)	V(2)−O(7)	2.337(3)	V(2)−O(4)	1.672(3)
Se(1)−O(6)	1.655(3)	V(2)−O(8)	1.971(3)	V(2)−O(2)	1.784(2)
		V(2)−O(9)	1.995(3)	V(2)−O(2)	1.784(2)
Se(2)−O(5)	1.734(3)	V(2)−O(10)	2.186(3)		
Se(2)−O(5)	1.734(3)			Se(1)−O(6)	1.655(3)
Se(2)−O(7)	1.677(4)	Se(1)−O(4)	1.749(3)	Se(1)−O(3)	1.734(2)
		Se(1)−O(10)	1.713(3)	Se(1)−O(3)	1.734(2)
		Se(1)−O(11)	1.666(3)		
		Se(2)−O(8)	1.719(3)		
		Se(2)−O(9)	1.738(3)		
		Se(2)−O(13)	1.661(3)		
		Se(3)−O(12)	1.676(3)		
		Se(3)−O(5)	1.706(3)		
		Se(3)−O(3)	1.724(3)		

TG/DTA 6300 series (SII Nano Technology Inc.). Approximately 20 mg of the samples were placed into a platinum crucible and heated and cooled between RT and 900 °C under nitrogen gas flowing at a rate of 10 °C min^{-1} (see Supporting Information, Figure S4).

Second-Harmonic Generation. Powder SHG measurements were performed on a modified Kurtz −NLO system using a pulsed Nd:YAG laser with a wavelength of 1064 nm. A detailed description of the equipment and methodology has been published elsewhere.[66] As the powder SHG efficiency has been shown to depend strongly on particle size,[67] the $A_4(VO_2)_2(SeO_3)_4(Se_2O_5)$ (A = Sr^{2+} or Pb^{2+}) materials were ground and sieved into distinct particle size ranges (<20, 20−45, 45−63, 63−75, 75−90, >90 μm). Relevant comparisons with known SHG materials were made by grinding and sieving crystalline α−SiO_2 and $LiNbO_3$ into the same particle size ranges. No index matching fluid was used in any of the experiments (see Supporting Information, Figure S5).

Piezoelectric Measurements. Converse piezoelectric measurements were performed using a Radiant Technologies RT66A piezoelectric test system with a TREK high voltage amplifier, Precision Materials Analyzer, Precision High Voltage Interface, and MTI 2000 Fotonic Sensor. The samples of $Sr_4(VO_2)_2(SeO_3)_4(Se_2O_5)$ and $Pb_4(VO_2)_2(SeO_3)_4(Se_2O_5)$ were pressed into pellets (~1.3 cm diameter, ~1 mm thickness) and sintered at 400 and 300 °C for 3 days, respectively. Silver paste was applied to both sides of the pellets, and the pellets were cured at 300 °C for 12 h. The same pellets were also used in polarization measurements (see Supporting Information, Figure S6).

Polarization Measurements. The polarization was measured on a Radiant Technologies RT66A ferroelectric test system with a TREK high voltage amplifier between RT and 215 °C in a Delta 9023 environmental test chamber. The unclamped pyroelectric coefficient, defined as dP/dT (change in polarization with respect to the change in temperature), was determined by measuring the polarization as a function of temperature. A detailed description of the methodology used has been published elsewhere.[66] To measure any possible ferroelectric behavior, the polarization was measured at RT under a static electric field of 700 V/cm between 50−200 Hz. For the pyroelectric measurements, the polarization was measured statically from RT to 215 °C in 10 °C increments, with an electric field of 700 V/cm. The temperature was allowed to stabilize before the polarization was measured (see Supporting Information, Figures S7 to S9). For all of the structural figures and electronic structure results, the program VESTA was used.[68]

Table 3. Selected Bond Distances (Å) for $Sr_4(VO_2)_2(SeO_3)_4(Se_2O_5)$ and $Pb_4(VO_2)_2(SeO_3)_4(Se_2O_5)$

$Sr_4(VO_2)_2(SeO_3)_4(Se_2O_5)$		$Pb_4(VO_2)_2(SeO_3)_4(Se_2O_5)$	
V(1)−O(1)	1.624(4)	V(1)−O(1)	1.611(7)
V(1)−O(2)	1.632(4)	V(1)−O(2)	1.649(8)
V(1)−O(3)	1.944(4)	V(1)−O(3)	1.948(7)
V(1)−O(4)	1.999(4)	V(1)−O(4)	1.973(7)
V(1)−O(5)	2.020(4)	V(1)−O(5)	1.986(7)
Se(1)−O(4)	1.719(4)	Se(1)−O(4)	1.724(7)
Se(1)−O(5)	1.711(4)	Se(1)−O(5)	1.707(7)
Se(1)−O(6)	1.663(4)	Se(1)−O(6)	1.637(7)
Se(2)−O(3)	1.711(4)	Se(2)−O(3)	1.707(7)
Se(2)−O(10)	1.701(4)	Se(2)−O(10)	1.686(7)
Se(2)−O(11)	1.690(3)	Se(2)−O(11)	1.698(6)
Se(3)−O(7)	1.652(4)	Se(3)−O(7)	1.641(7)
Se(3)−O(8)	1.672(4)	Se(3)−O(8)	1.688(8)
Se(3)−O(9)	1.806(3)	Se(3)−O(9)	1.807(5)

RESULTS AND DISCUSSION

Structures. $Ca_2(VO_2)_2(SeO_3)_3(H_2O)_2$ exhibits a one-dimensional crystal structure consisting of edge- or corner-shared VO_6 octahedra and SeO_3 polyhedra (see Figure 1). The edge-shared binuclear V_2O_{10} units bridged by two $Se(1)O_3$ polyhedra are connected through $Se(2)O_3$ polyhedra, that create a one-dimensional chain along the *b*-axis. These chains are separated by Ca^{2+} cations and water molecules. In connectivity terms, the material may be written as $\{2[VO_{5/2}O_{1/1}]^{2-}$ $2[Se(1)O_{2/2}O_{1/1}]^0$ $[Se(2)O_{2/2}O_{1/1}]^0\}^{4-}$, with charge balance maintained by two Ca^{2+} cations. The crystallographically unique V^{5+} cation is found in a distorted octahedral coordination environment, attributable to SOJT effects, with V−O distances ranging between 1.597(3)−2.248(3) Å. The Se^{4+} cations are in highly asymmetric coordination environments attributable to their stereo-active lone-pair, and are bonded to three oxygen atoms with Se−O distances ranging from 1.718(3)−1.748(3) Å. The Ca^{2+} cation is surrounded by eight oxygen atoms with Ca−O distances between 2.405(3)−2.583(3) Å. Bond valence calculations[69,70] resulted in values of 5.07, 3.90−4.00, and 2.07 for V^{5+}, Se^{4+}, and Ca^{2+}, respectively. Detailed bond valence calculation results for $Ca_2(VO_2)_2(SeO_3)_3(H_2O)_2$ are shown in Supporting Information, Table S6.

$Sr_2(VO_2)_2(SeO_3)_3$ exhibits a two-dimensional crystal structure consisting of edge- or corner-shared VO_6 octahedra, VO_5 square pyramids, and SeO_3 polyhedra (see Figure 2). Layers of $[V_2Se_3O_{13}]^{2-}$ anions stack along the *a*-axis, and are separated by the Sr^{2+} cations. Interestingly, the layer is composed of two parts: arrays consisting of VO_5 and SeO_3 polyhedra and binuclear V_2O_{10} units bridged by two $Se(2)O_3$ polyhedra (see Figure 3). The former lies in the *bc*-plane, and is connected by the latter through two $Se(1)O_3$ polyhedra. This linkage results in a zigzag array along the *b*-axis as seen in Figure 2b.

dx.doi.org/10.1021/ic2021403 | Inorg. Chem. 2012, 51, 609−619

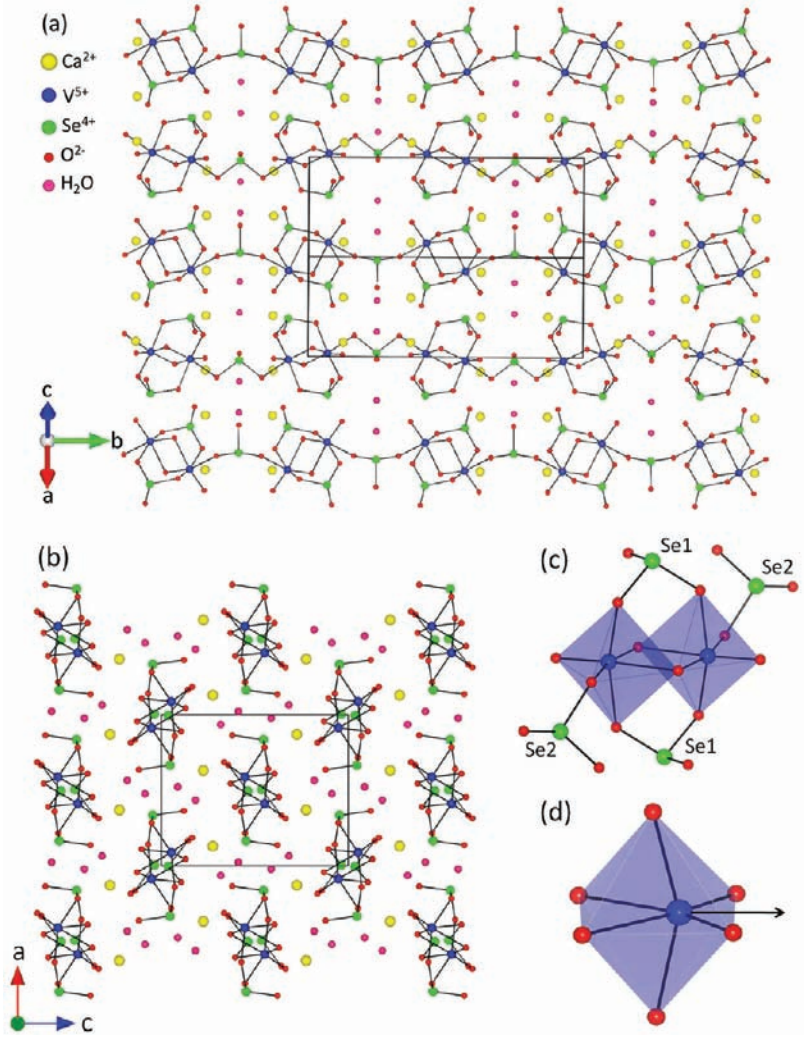

Figure 1. Ball-and-stick and polyhedral diagrams of the $Ca_2(VO_2)_2(SeO_3)_3(H_2O)_2$ structure in the (a) *bc*- and (b) *ac*-plane, and (c) shows the dimeric unit consisting of two VO_6 octahedra. An off-center distortion of the V^{5+} cation (C_2-type) is shown in (d). The black arrow in (d) represents the distortion direction of the V^{5+} cation.

In connectivity terms, the materials may be written as $\{[V(1)O_{3/2}O_{2/1}]^{2-}$ $[V(2)O_{5/2}O_{1/1}]^{2-}$ $[Se(1)O_{2/2}O_{1/1}]^0$ $[Se(2)O_{2/2}O_{1/1}]^0$ $[Se(3)O_{2/2}O_{1/1}]^0\}^{4-}$, with the charge balance maintained by two Sr^{2+} cations. The $V(1)^{5+}$ cation is observed in a distorted square pyramidal coordination environment with V(1)−O bond distances between 1.612(3)−2.005(3) Å, whereas the $V(2)^{5+}$ cation is found in a distorted octahedral environment, attributable to SOJT effects, with V(2)−O bond distances ranging from 1.612(3) Å to 2.337(3) Å. The three Se^{4+} cations are found in highly asymmetric coordination environments attributable to their stereo-active lone-pair, and are bonded to three oxygen atoms with Se−O bond distances of 1.661(3)−1.749(3) Å. The Sr^{2+} cation is surrounded by eight oxygen atoms with Sr−O distances ranging between 2.494(3)−2.761(3) Å. Bond valence calculations resulted in values of 4.80−4.92, 3.92−3.98, and 1.91−2.14 for V^{5+}, Se^{4+}, and Sr^{2+}, respectively. Detailed bond valence calculation results for $Sr_2(VO_2)_2(SeO_3)_3$ are shown in Supporting Information, Table S7.

One of the interesting structural features is that the same binuclear V_2O_{10} unit, that is, a dimer consisting of two edge-shared VO_6 octahedra bridged by two SeO_3 polyhedra, is found in $Ca_2(VO_2)_2(SeO_3)_3(H_2O)_2$ and $Sr_2(VO_2)_2(SeO_3)_3$ (see Figures 1c and 3b). Two VO_6 octahedra are edge-shared to form a V_2O_{10} dimer, are bridged by two SeO_3 polyhedra through four oxygen atoms, and are linked to other structural units through two SeO_3 polyhedra leaving one oxygen atom as a terminal ligand. This connectivity results in a C_2-type distortion (toward an edge) with two short, two middle, and two long V−O bond distances (see Figures 1d and 3d). Although anhydrous $Ca_2(VO_2)_2(SeO_3)_3(H_2O)_2$, that is, $Ca_2(VO_2)_2(SeO_3)_3$, has a similar stoichiometry to $Sr_2(VO_2)_2(SeO_3)_3$, the structural dimensions are different. This is likely attributable to the presence of the water molecules in $Ca_2(VO_2)_2(SeO_3)_3(H_2O)_2$ and the occurrence of the VO_5 square pyramids in $Sr_2(VO_2)_2(SeO_3)_3$. Recall that in $Ca_2(VO_2)_2(SeO_3)_3(H_2O)_2$, the V^{5+} cation is solely in an octahedral coordination environment. The water molecules residing between the one-dimensional chains with the Ca^{2+} cations in $Ca_2(VO_2)_2(SeO_3)_3(H_2O)_2$ restrict the inter-chain connection, whereas the VO_5 square pyramid in $Sr_2(VO_2)_2(SeO_3)_3$ acts as a linker to form a higher dimensional, that is, two-dimensional, crystal structure. We attempted to dehydrate $Ca(VO_2)_2(SeO_3)_3(H_2O)_2$ to investigate any structural transition to the $Sr_2(VO_2)_2(SeO_3)_3$ structure. The Ca-phase was heated to 250 °C for several hours to remove all of

dx.doi.org/10.1021/ic2021403 | *Inorg. Chem.* 2012, 51, 609−619

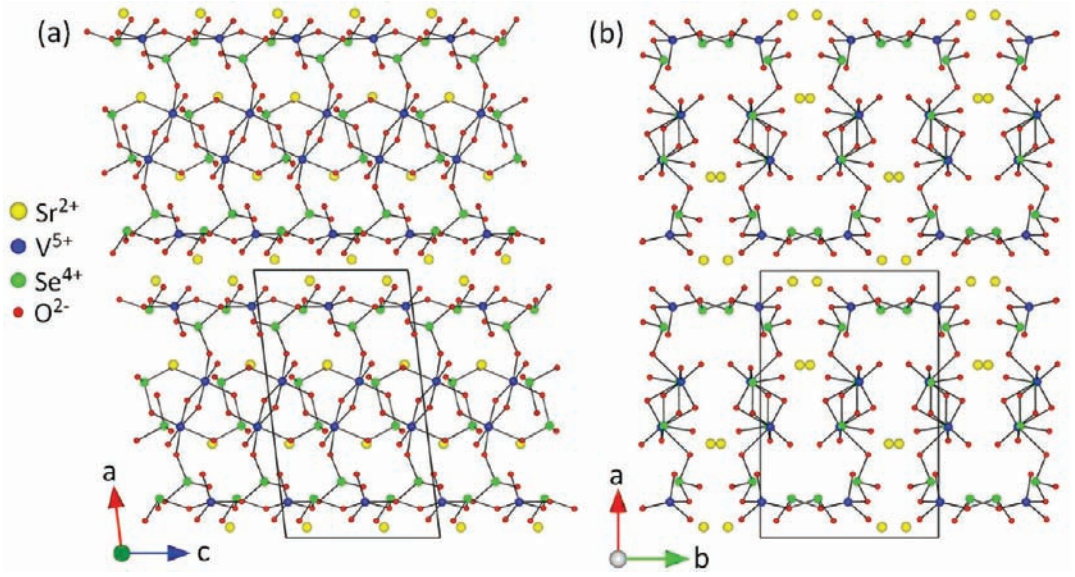

Figure 2. Ball-and-stick diagram of the $Sr_2(VO_2)_2(SeO_3)_3$ structure in the (a) *ac*- and (b) *ab*-plane. The structure exhibits two-dimensional layers consisting of zigzag arrays along the *b*-axis.

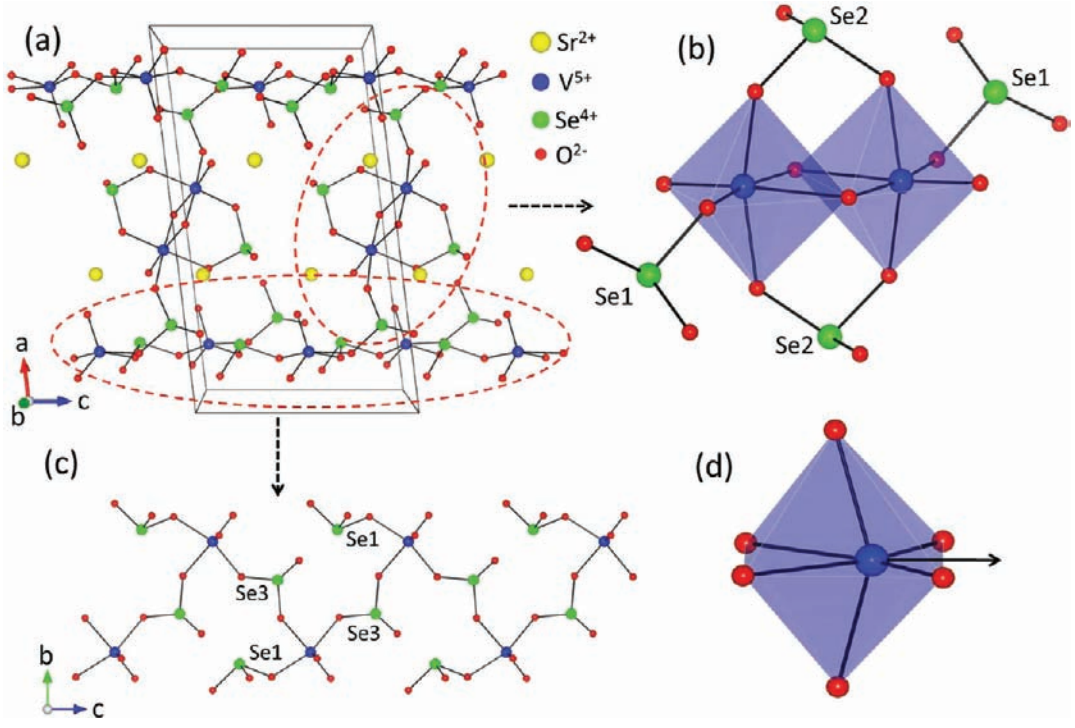

Figure 3. Ball-and-stick and polyhedral diagrams of a part of the $Sr_2(VO_2)_2(SeO_3)_3$ structure in the (a) *ac*-plane, and two different structural units of (b) and (c). An off-center distortion of the V^{5+} cation (C_2-type) is shown in (d). The black arrow in (d) represents the distortion direction of the V^{5+} cation.

the H_2O molecules. The powder XRD pattern after the attempted dehydration was the same as before, indicating that a structural transition did not occur (see Supporting Information, Figure S1).

$Ba(V_2O_5)(SeO_3)$ also exhibits a two-dimensional crystal structure consisting of edge- or corner-shared VO_6 octahedra, VO_4 tetrahedra, and SeO_3 polyhedra (see Figure 4). Puckered layers of $[V_2SeO_8]^{2-}$ anions stack along the *a*-axis, and are separated by the Ba^{2+} cations. The distorted $V(1)O_6$ octahedra are bridged by the $V(2)O_4$ and SeO_3 polyhedra along the *b*-axis, and is further connected by the $V(2)O_4$ tetrahedra along the *c*-axis forming the two-dimensional layer. In connectivity terms, the material may be written as $\{[V(1)O_{5/2}O_{1/1}]^{2-}\ [V(2)O_{3/2}O_{1/1}]^0\ [Se(1)O_{2/2}O_{1/1}]^0\}^{2-}$, with the charge balance maintained by one Ba^{2+} cation. The $V(1)^{5+}$ cation is found in a distorted octahedral coordination environment, attributable to SOJT effects, with V(1)−O bond distances ranging between 1.588(3)−2.278(3) Å. Also, the distortion direction of the V^{5+} cation is toward a corner, that is, a C_4-type distortion. Since five oxide ligands in the $V(1)O_6$ octahedron are shared by three $V(2)O_4$ and two SeO_3 polyhedra, the $V(1)^{5+}$ cation prefers to shift toward its corner, that is, a terminal ligand, resulting in one

dx.doi.org/10.1021/ic2021403 | *Inorg. Chem.* 2012, 51, 609−619

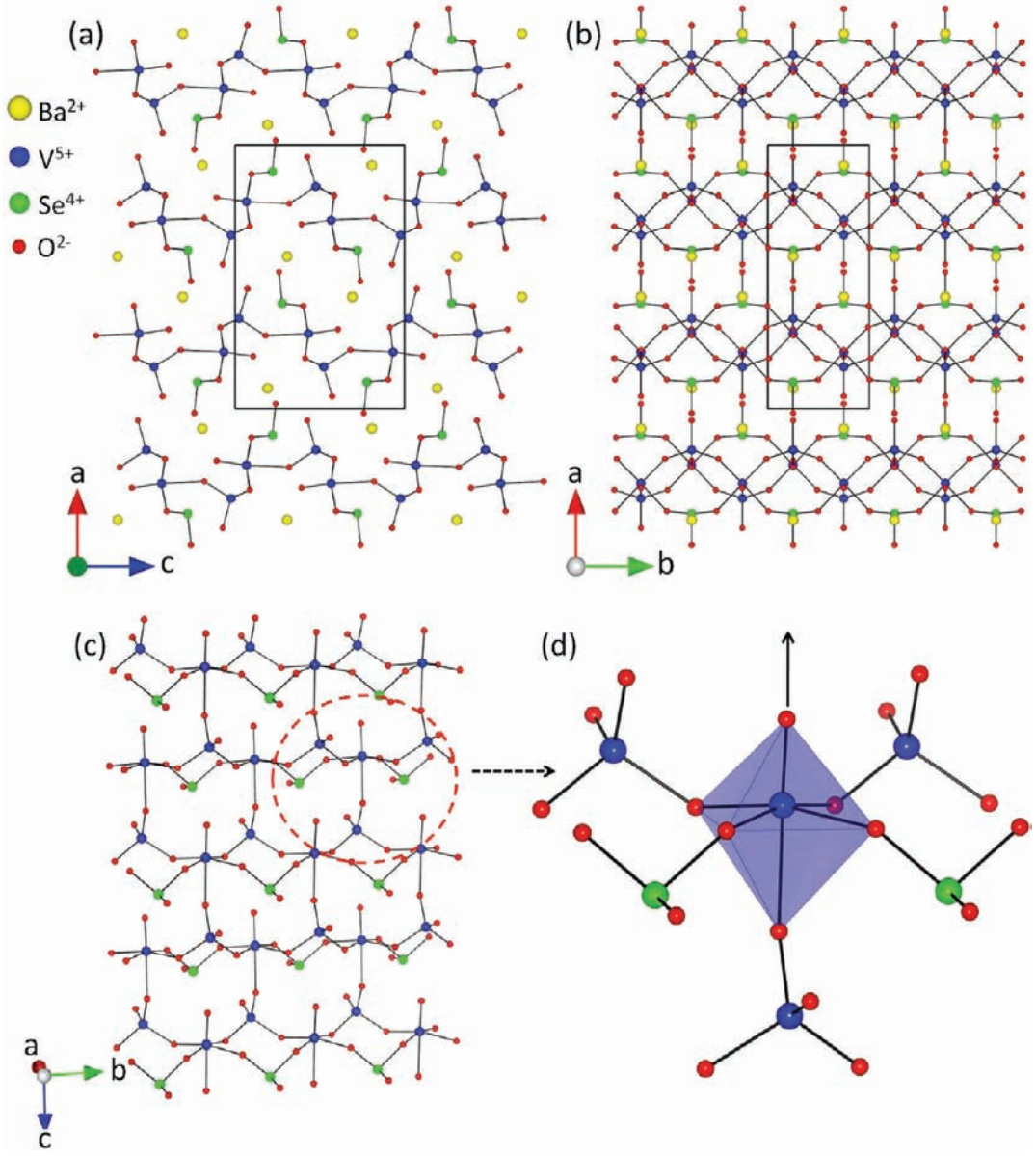

Figure 4. Ball-and-stick and polyhedral diagrams of a part of the $Ba(V_2O_5)(SeO_3)$ structure in the (a) *ac*-, (b) *ab*-, and (c) *bc*-plane. An off-center distortion of the V^{5+} cation (C_4-type) is shown in (d). The black arrow in (d) represents the distortion direction of the V^{5+} cation.

short, one long, and four normal V(1)−O bond distances (see Figure 4d). The V(2)−O bond distances in the $V(2)O_4$ tetrahedron range from 1.626(3) Å to 1.784(2) Å. The Se^{4+} cation is found in a highly asymmetric coordination environment attributable to its stereo-active lone-pair with Se−O bond distances of 1.655(3)−1.734(2) Å. The Ba^{2+} cation is surrounded by 10 oxygen atoms with Ba−O distances between 2.713(3) Å and 3.063(2) Å. Bond valence calculations resulted in values of 5.01−5.13, 3.98, and 2.02 for V^{5+}, Se^{4+}, and Ba^{2+}, respectively. Detailed bond valence calculation results for $Ba(V_2O_5)(SeO_3)$ are shown in Supporting Information, Table S8.

The tellurium analogue of $Ba(V_2O_5)(SeO_3)$ (or BaV_2SeO_8) has been reported, BaV_2TeO_8;[71] however, its crystal structure is different from the selenium phase. BaV_2TeO_8 exhibits a one-dimensional crystal structure composed of edge-shared VO_5, VO_4, and TeO_4 polyhedra. Also, dimeric V_2O_8 (two edge-shared VO_5 square pyramids) units connected by the VO_4 and TeO_4 polyhedra are observed. The discrepancy, between the selenite and tellurite, is thought to be attributable to the occurrence of the VO_6 and the SeO_3 polyhedra in BaV_2SeO_8 and the presence of the VO_5 and the TeO_4 polyhedra in BaV_2TeO_8. Thus, the materials may also be described as $Ba(V_2O_5)(SeO_3)$ and $Ba(V_2O_4)(TeO_4)$, respectively.

$Sr_4(VO_2)_2(SeO_3)_4(Se_2O_5)$ and $Pb_4(VO_2)_2(SeO_3)_4(Se_2O_5)$ are iso-structural, and exhibit one-dimensional crystal structures consisting of corner-shared VO_5 and SeO_3 polyhedra (see Figure 5). The VO_5 square pyramid is surrounded by three SeO_3 polyhedra, and bridged by $Se(1)O_3$ polyhedra forming a one-dimensional chain (see Figure 6). Also, these chains are found perpendicular to each other, and are separated by the Sr^{2+} or Pb^{2+} cations and $[Se_2O_5]^{2-}$ groups. In connectivity terms, the materials may be written as $\{2[VO_{3/2}O_{2/1}]^{2-}$ $2[Se(1)O_{2/2}O_{1/1}]^0$ $2[Se(2)O_{1/2}O_{2/1}]^{1-}$ $2[Se(3)O_{1/2}O_{2/1}]^{1-}\}^{8-}$, with the charge balance maintained by four Sr^{2+} or Pb^{2+} cations. The crystallographically unique V^{5+} cation is found in a

dx.doi.org/10.1021/ic2021403 | *Inorg. Chem.* 2012, 51, 609−619

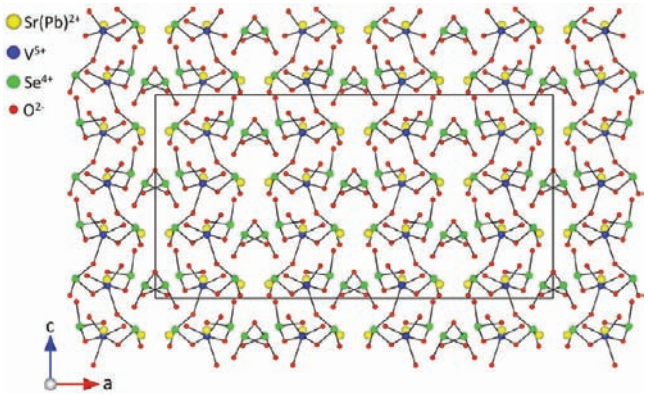

Figure 5. Ball-and-stick diagram of the $A_4(VO_2)_2(SeO_3)_4(Se_2O_5)$ (A = Sr^{2+} or Pb^{2+}) structure in the *ac*-plane. Isolated Se_2O_5 groups are found between the one-dimensional chains.

distorted square pyramidal coordination environment with V−O distances of 1.611(7) Å−2.020(4) Å. All of the Se^{4+} cations are in highly asymmetric coordination environments attributable to their stereo-active lone-pair, and are bonded to three oxygen atoms with Se−O bond distances ranging from 1.641(7) Å to 1.807(5) Å. The most interesting structural feature is that isolated Se_2O_5 groups are found in the crystal structure. In fact, the Se_2O_5 group usually acts as a bridging ligand between the MO_x polyhedra.[72−74] In our effort to find the materials containing this isolated Se_2O_5 group, only a few compounds, for example, $A_2(Se_2O_5)$ (A = K^+, or NH_4^+)[75,76] or $B(Se_2O_5)$ (B = alkaline earth metals or Pb^{2+}),[77−81] could be found. Thus, $A_4(VO_2)_2(SeO_3)_4(Se_2O_5)$ (A = Sr^{2+} or Pb^{2+}) are very rare examples in the solid-state oxide materials that possess an isolated Se_2O_5 group. The Sr^{2+} and Pb^{2+} cations are surrounded by 9 to 11 oxygen atoms with Sr(Pb)−O distances between 2.661(4) Å and 3.079(7) Å. This similar coordination environment implies that the lone-pair on the Pb^{2+} cation may be regarded as inert rather than stereo-active. Bond valence calculations resulted in values of 5.04−5.11, 3.99−4.19, and 1.88−1.91 for V^{5+}, Se^{4+}, and Sr^{2+} or Pb^{2+}, respectively. Detailed bond valence calculation results for $A_4(VO_2)_2(SeO_3)_4(Se_2O_5)$ (A = Sr^{2+} or Pb^{2+}) are shown in Supporting Information, Table S9.

Local Dipole Moments, Octahedral Distortions, BSI, and GII Calculations. Local dipole moments[82,83] were calculated on the reported materials and are summarized in Table 4. For all materials, the dipole moment is attributable to the asymmetric polyhedra, that is, the distorted VO_6 and SeO_3 polyhedra. For centrosymmetric materials, $Ca_2(VO_2)_2(SeO_3)_3(H_2O)_2$, $Sr_2(VO_2)_2(SeO_3)_3$, and $Ba(V_2O_5)(SeO_3)$, although individual dipole moments are observed, the net polarization is zero, as the individual moments are pointed in opposite directions. For $A_4(VO_2)_2(SeO_3)_4(Se_2O_5)$ (A = Sr^{2+} or Pb^{2+}), however, the situation is different, as the materials are macroscopically polar. There are three kinds of SeO_3 polyhedra that exhibit comparable dipole moment magnitudes. The polarization associated with the $Se(1)O_3$ polyhedra results in a net dipole moment approximately along the [0 0 −1] direction, whereas the net dipole moment from the $Se(2)O_3$ polyhedra points in the approximate [0 0 1] direction. Thus the polarization associated with $Se(1)O_3$ and $Se(2)O_3$ are pointed in opposite directions (see Figure 7). The $Se(3)_2O_5$ group is composed of two corner-shared SeO_3 polyhedra. These polyhedra are pointed in the same direction, and thus produce a net dipole moment. This polarization is toward the approximate [0 0 −1] direction and is responsible for the macroscopic polarization in $A_4(VO_2)_2(SeO_3)_4(Se_2O_5)$ (A = Sr^{2+} or Pb^{2+}). Thus the functional properties associated with the polarization of $A_4(VO_2)_2(SeO_3)_4(Se_2O_5)$ (A = Sr^{2+} or Pb^{2+}) may be attributed to these Se_2O_5 groups. In addition to dipole moment calculations, we used a continuous symmetry measures methodology[84−86] to calculate the magnitude of the V^{5+} distortion. Using the SHAPE program,[87] we determined that the magnitude of the intra-octahedral distortion for the V^{5+} cation in $Ca_2(VO_2)_2(SeO_3)_3(H_2O)_2$, $Sr_2(VO_2)_2(SeO_3)_3$, and $Ba(V_2O_5)(SeO_3)$ is 0.162, 0.188, and 0.076 $Å^2$ respectively. These values are consistent with earlier reports,[88] as well as the magnitude of the dipole moment. Larger dipole moments are observed in cations with a larger magnitude of distortion (see Table 4). In addition to the local dipole moment and distortion calculations, bond strain[89] and global instability[90] indices, BSI and GII respectively, were calculated. These indices are an extension of bond valence concepts and are indicative of electronic and lattice-induced strains. BSI and GII values greater than 0.05 vu (valence unit) reveal that the structure is strained. For $Ca_2(VO_2)_2(SeO_3)_3(H_2O)_2$, $Sr_2(VO_2)_2(SeO_3)_3$, and $Ba(V_2O_5)(SeO_3)$, the BSI values are substantially greater than GII values indicating electronic strains are stronger than lattice-induced strains (see Table 4). This is reasonable as both V^{5+} and Se^{4+} cations undergo SOJT distortions. With $A_4(VO_2)_2(SeO_3)_4(Se_2O_5)$ (A = Sr^{2+} or Pb^{2+}), however, the BSI and GII values are comparable. This is not surprising as only Se^{4+} cations can undergo a SOJT distortion. The V^{5+} cations, in these materials, cannot undergo SOJT distortions attributable to their square pyramidal coordination environment.

Infrared Spectroscopy. The infrared spectra for the reported materials revealed V−O and Se−O vibrations between 400 and 4000 cm^{-1}. For $Ca_2(VO_2)_2(SeO_3)_3(H_2O)_2$, the band around 3500 cm^{-1} occurs attributable to O−H vibrations in the water molecules. For all materials, the bands observed in 850−600 cm^{-1} and 550−400 cm^{-1} can be attributed to V−O and O−V−O vibrations, respectively, whereas the bands in 900−850 cm^{-1} can be attributed to Se−O vibrations. The assignments are consistent with those previously reported[47,50,57] (see Supporting Information, Figure S2).

UV−vis Diffuse Reflectance Spectroscopy. The UV−vis diffuse reflectance spectra indicate the absorption energy for the materials is between 2.13 and 3.37 eV. Absorption (*K*/*S*) data were calculated from the Kubelka−Munk function:[65]

$$F(R) = \frac{(1-R)^2}{2R} = \frac{K}{S}$$

with *R* representing the reflectance, *K* the absorption, and *S* the scattering. In a *K*/*S* versus *E* (eV) plot, extrapolating the linear part of the rising curve to zero provides the onset of absorption at 3.08, 2.96, 2.13, 2.66, and 3.37 eV for $Ca_2(VO_2)_2(SeO_3)_3(H_2O)_2$, $Sr_2(VO_2)_2(SeO_3)_3$, $Ba(V_2O_5)(SeO_3)$, $Sr_4(VO_2)_2(SeO_3)_4(Se_2O_5)$, and $Pb_4(VO_2)_2(SeO_3)_4(Se_2O_5)$, respectively. The UV−vis diffuse reflectance spectra have been deposited in Supporting Information, Figure S3.

Thermal Analyses. The thermal behavior of the reported materials was investigated using thermogravimetric analysis (TGA) and differential thermal analysis (DTA). None of materials are stable up to 900 °C attributable to the sublimation of SeO_2. The decompositions start at approximately 330, 420, 330, 440, and 305 °C corresponding to the SeO_2 sublimation

dx.doi.org/10.1021/ic2021403 | *Inorg. Chem.* 2012, 51, 609−619

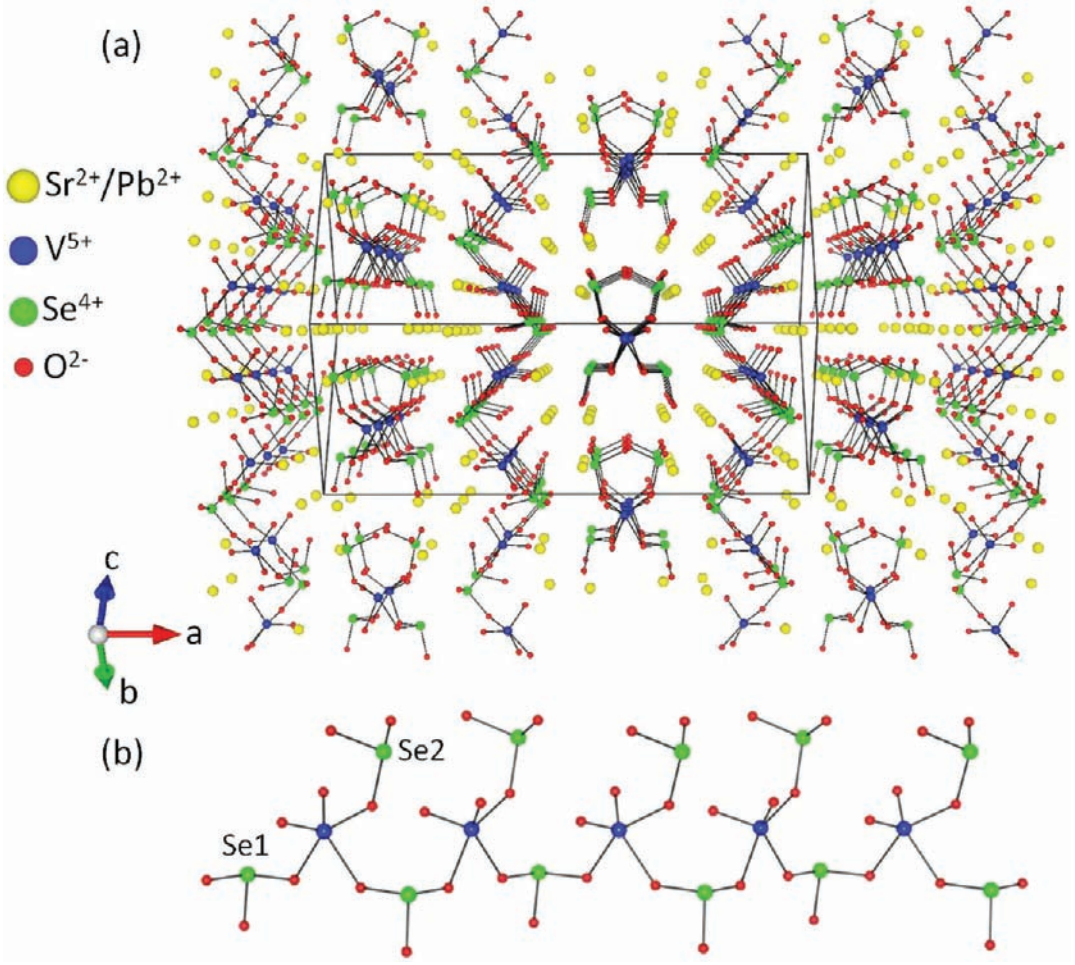

Figure 6. (a) Ball-and-stick diagram of the $A_4(VO_2)_2(SeO_3)_4(Se_2O_5)$ (A = Sr^{2+} or Pb^{2+}) structure indicating one-dimensional chains. A part of the one-dimensional chain is seen in (b). For the sake of clarity, the Se_2O_5 groups have been removed.

Table 4. Dipole Moments, Octahedral Distortion Magnitudes (Δ_0 in Å^2), BSI and GII values, for $Ca_2(VO_2)_2(SeO_3)_3(H_2O)_2$, $Sr_2(VO_2)_2(SeO_3)_3$, $Ba(V_2O_5)(SeO_3)$, $Sr_4(VO_2)_2(SeO_3)_4(Se_2O_5)$, and $Pb_4(VO_2)_2(SeO_3)_4(Se_2O_5)$, and SHG Efficiency (Relative to α−SiO_2), Piezoelectric Response (pm/V), and Pyroelectric Coefficient (μC/m^2·K at 70 °C) for $Sr_4(VO_2)_2(SeO_3)_4(Se_2O_5)$, and $Pb_4(VO_2)_2(SeO_3)_4(Se_2O_5)$

	dipole moments									
compounds	$V^{5+}O_4$	$V^{5+}O_5$	$V^{5+}O_6$	Se^{4+}	Δ_0	BSI	GII	SHG	Piezo. d_{33}	Pyro. Coeff.
$Ca_2(VO_2)_2(SeO_3)_3(H_2O)_2$			9.97	6.75−7.26	0.162	0.137	0.093			
$Sr_2(VO_2)_2(SeO_3)_3$		1.79	10.6	6.47−8.46	0.188	0.189	0.124			
$Ba(V_2O_5)(SeO_3)$	1.76		4.48	8.21	0.076	0.145	0.089			
$Sr_4(VO_2)_2(SeO_3)_4(Se_2O_5)$		3.33		6.58−9.04		0.071	0.077	130	43	−27
$Pb_4(VO_2)_2(SeO_3)_4(Se_2O_5)$		2.64		6.89−8.79		0.091	0.084	150	53	−42

for $Ca_2(VO_2)_2(SeO_3)_3(H_2O)_2$, $Sr_2(VO_2)_2(SeO_3)_3$, $Ba(V_2O_5)(SeO_3)$, $Sr_4(VO_2)_2(SeO_3)_4(Se_2O_5)$, and $Pb_4(VO_2)_2(SeO_3)_4(Se_2O_5)$, respectively. However, for $Ca_2(VO_2)_2(SeO_3)_3(H_2O)_2$, an additional step is observed at ∼120−220 °C attributable to dehydration of two water molecules. The endothermic peaks in the heating cycles of DTA curves indicate the decomposition of the materials, and the exothermic peaks in the cooling cycles are attributable to recrystallization of the residues after the decomposition. The residues are $Ca_2V_2O_7$[91] for $Ca_2(VO_2)_2(SeO_3)_3(H_2O)_2$, $Sr_2V_2O_7$[92] for $Sr_2(VO_2)_2(SeO_3)_3$, BaV_2O_6,[93] $Ba_3V_4O_{13}$,[94] and unidentified phases for $Ba(V_2O_5)(SeO_3)$, $Sr_3V_2O_8$,[95] SrV_2O_6,[96] and unidentified phases for $Sr_4(VO_2)_2(SeO_3)_4(Se_2O_5)$, and $Pb_4V_2O_9$[97] for $Pb_4(VO_2)_2(SeO_3)_4(Se_2O_5)$, respectively. The experimental weight loss is in good agreement with the calculated weight loss. TGA and DTA data are given in Supporting Information, Figure S4.

Second-Harmonic Generation (SHG) and Piezoelectricity. As $Sr_4(VO_2)_2(SeO_3)_4(Se_2O_5)$ and $Pb_4(VO_2)_2(SeO_3)_4(Se_2O_5)$ crystallize in a NCS space group, *Fdd*2, their SHG and piezoelectric phenomena could be investigated. Through powder SHG measurements, using 1064 nm radiation, the SHG efficiencies for $Sr_4(VO_2)_2(SeO_3)_4(Se_2O_5)$ and $Pb_4(VO_2)_2(SeO_3)_4(Se_2O_5)$ are approximately 130 and 150 × α−SiO_2 respectively in the 45−63 μm particle size range. These SHG efficiencies are thought to be attributable to the parallel alignment of dipole moments driven by the asymmetric

dx.doi.org/10.1021/ic2021403 | *Inorg. Chem.* 2012, 51, 609−619

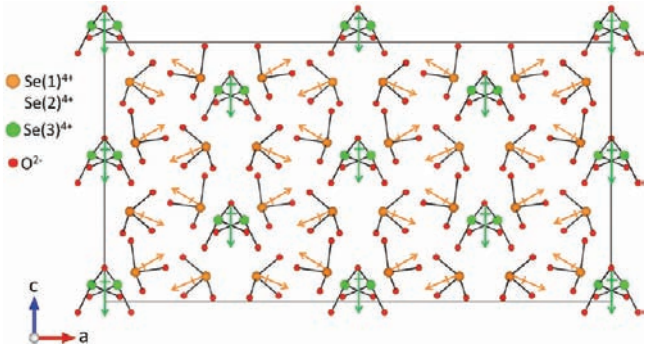

Figure 7. Dipole moment directions associated with SeO_3 polyhedra in the $A_4(VO_2)_2(SeO_3)_4(Se_2O_5)$ (A = Sr^{2+} or Pb^{2+}) along the *b*-axis. Note that only dipole moments from Se_2O_5 groups (green arrows) are aligned in the same direction and others (brown arrows) are nearly canceled. For the sake of clarity, Sr^{2+} or Pb^{2+} and V^{5+} cations are removed.

$Se(3)_2O_5$ groups. Although $Se(1)O_3$ and $Se(2)O_3$ polyhedra also exhibit individual dipole moment, their contribution to SHG is minimal attributable to their anti-parallel alignment. Also, the VO_5 polyhedra does not contribute significantly to the SHG efficiency, as the V^{5+} cation cannot undergo a SOJT distortion attributable to its square pyramidal coordination environment. Additional SHG measurements with various particle sizes indicate that both materials exhibit non-phase-matching behavior (type I), and fall into the class C category of SHG materials (see Supporting Information, Figure S5).[67] The average NLO susceptibilities, $\langle d_{eff}\rangle_{exp}$, could be determined resulting in values of 6.3 and 6.8 pm/V for $Sr_4(VO_2)_2(SeO_3)_4(Se_2O_5)$ and $Pb_4(VO_2)_2(SeO_3)_4(Se_2O_5)$, respectively. Converse piezoelectric measurements were performed on both materials. Piezoelectric charge constants (d_{33}) of 43 and 53 pm/V for $Sr_4(VO_2)_2(SeO_3)_4(Se_2O_5)$ and $Pb_4(VO_2)_2(SeO_3)_4(Se_2O_5)$, respectively were determined (see Supporting Information, Figure S6).

Polarization Measurements. Since $Sr_4(VO_2)_2(SeO_3)_4(Se_2O_5)$ and $Pb_4(VO_2)_2(SeO_3)_4(Se_2O_5)$ are polar as well as NCS, we also measured their ferroelectric and pyroelectric properties. From the frequency dependent polarization measurements, it is evident that neither material is ferroelectric as the observed "loops" are attributable to dielectric loss and not ferroelectric hysteresis (see Supporting Information, Figure S7). It is important to understand why the materials are not ferroelectric, that is, the macroscopic polarization cannot be reversed under an external electric field. Recall that the macroscopic polarization in both materials is mainly attributable to the $Se(3)_2O_5$ groups. Thus any macroscopic polarization reversal will involve microscopic polarization reversal in the $Se(3)_2O_5$ group. Excluding the possibility of breaking Se−O bonds, one possible manner for polarization reversal is a rotation of the $Se(3)_2O_5$ groups. We suggest that this rotation would be energetically unfavorable as it involves a large movement of the Se^{4+} cations and oxygen atoms. In addition, an increase with the lone-pair−lone-pair repulsive interactions with other Se^{4+} cations near the $Se(3)^{4+}$ cation would occur. Another manner for polarization reversal to possibly occur is through an umbrella-type inversion of each $Se(3)O_3$ polyhedron in the $Se(3)_2O_5$ group. As we have demonstrated previously,[98] the barrier to inversion for a Se^{4+} cation is large in comparison with Ti^{4+} in ferroelectric materials such as $BaTiO_3$ and $PbTiO_3$.[99] Thus, for a variety of energetically unfavorable reasons neither $Sr_4(VO_2)_2(SeO_3)_4(Se_2O_5)$ or $Pb_4(VO_2)_2(SeO_3)_4(Se_2O_5)$ are ferroelectric. Pyroelectric measurements were performed on the reported materials (see Supporting Information, Figure S8 and S9). Pyroelectric coefficients, defined as a change in polarization as a function of temperature, were estimated to be of −27 and −42 $\mu C/m^2 \cdot K$ at 70 °C for $Sr_4(VO_2)_2(SeO_3)_4(Se_2O_5)$ and $Pb_4(VO_2)_2(SeO_3)_4(Se_2O_5)$, respectively. The electron localization function (ELF) isosurfaces with η = 0.9 for $Ba(V_2O_5)(SeO_3)$ is shown in Figure 8 where lobe-like isosurfaces are observed.

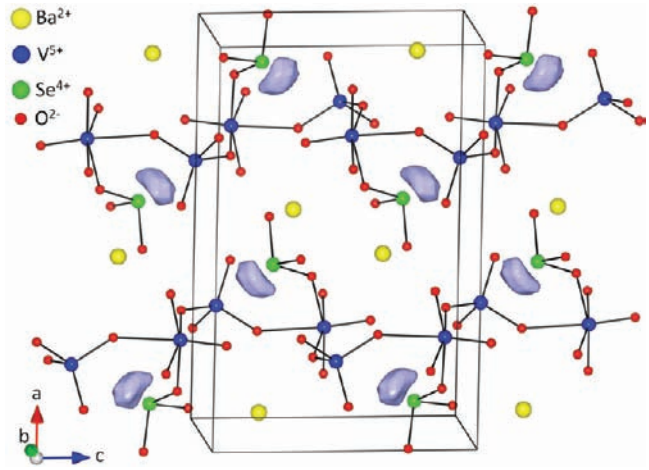

Figure 8. Visualization of the stereo-active lone-pair on the Se^{4+} cation through electron localization function (ELF) for $Ba(V_2O_5)(SeO_3)$ utilizing pseudopotential calculations. The lobe-like isosurfaces around the Se^{4+} cations indicate that the lone-pair is stereo-active.

Thus, the lone-pair on the Se^{4+} cation may be regarded as stereo-active.

CONCLUSION

We have successfully synthesized and characterized five new oxide materials, $Ca_2(VO_2)_2(SeO_3)_3(H_2O)_2$, $Sr_2(VO_2)_2(SeO_3)_3$, $Ba(V_2O_3)(SeO_3)$, $Sr_4(VO_2)_2(SeO_3)_4(Se_2O_5)$, and $Pb_4(VO_2)_2(SeO_3)_4(Se_2O_5)$. A structural diversity of the V^{5+} cation was observed through its various coordination environments, that is, tetrahedral, square pyramidal, and octahedral. Interestingly, $A_4(VO_2)_2(SeO_3)_4(Se_2O_5)$ (A = Sr^{2+} or Pb^{2+}) are NCS and polar and exhibit an isolated Se_2O_5 group. The moderate SHG efficiencies of these materials may be attributed to the parallel alignment of the Se_2O_5 groups. Although $A_4(VO_2)_2(SeO_3)_4(Se_2O_5)$ (A = Sr^{2+} or Pb^{2+}) are polar, the materials are not ferroelectric, that is, the observed polarization cannot be switched under an external electric field.

ASSOCIATED CONTENT

Supporting Information

X-ray data in CIF format, powder XRD patterns, IR and UV−vis spectra, TGA and DTA diagrams, piezoelectric and polarization loops, electronic band structure figures, and crystallographic data tables. This material is available free of charge via the Internet at http://pubs.acs.org.

AUTHOR INFORMATION

Corresponding Author

*E-mail: psh@uh.edu.

■ ACKNOWLEDGMENTS

We thank the Robert A. Welch Foundation (Grant E-1457) and the Texas Center for Superconductivity for support. We also acknowledge Prof. Miquel Llunell at Universitat de Barcelona for assistance in obtaining the SHAPE calculation data. J.Y. thanks International Centre for Diffraction Data for a 2011 Ludo Frevel Crystallography Scholarship Award.

■ REFERENCES

(1) Auciello, O.; Scott, J. F.; Ramesh, R. *Phys. Today* **1998**, *51*, 22.
(2) Haertling, G. H. *J. Am. Ceram. Soc.* **1999**, *82*, 797.
(3) Lang, F. S. B.; Das-Gupta, D. K. In *Handbook of Advanced Electronic and Photonic Materials and Devices*; Nalwa, H. S., Ed.; Academic Press: San Francisco, CA, 2001; Vol. *4*, p 1.
(4) Cady, W. G. *Piezoelectricity; an Introduction to the Theory and Applications of Electromechanical Phenomena in Crystals*; Dover: New York, 1964.
(5) Rieckhoff, K. E.; Peticolas, W. L. *Science* **1965**, *147*, 610.
(6) Chi, E. O.; Ok, K. M.; Porter, Y.; Halasyamani, P. S. *Chem. Mater.* **2006**, *18*, 2070.
(7) Hahn, T. *International Tables for Crystallography*; Kluwer Academic: Dordrecht, The Netherlands, 2006; Vol. *A*, Space Group Symmetry.
(8) Heier, K. R.; Norquist, A. J.; Halasyamani, P. S.; Duarte, A.; Stern, C. L.; Poeppelmeier, K. R. *Inorg. Chem.* **1999**, *38*, 762.
(9) Welk, M. E.; Norquist, A. J.; Stern, C. L.; Poeppelmeier, K. R. *Inorg. Chem.* **2000**, *39*, 3946.
(10) Welk, M. E.; Norquist, A. J.; Stern, C. L.; Poeppelmeier, K. R. *Inorg. Chem.* **2001**, *40*, 5479.
(11) Welk, M. E.; Norquist, A. J.; Arnold, F. P.; Stern, C. L.; Poeppelmeier, K. R. *Inorg. Chem.* **2002**, *41*, 5119.
(12) Marvel, M. R.; Lesage, J.; Baek, J.; Halasyamani, P. S.; Stern, C. L.; Poeppelmeier, K. R. *J. Am. Chem. Soc.* **2007**, *129*, 13963.
(13) Marvel, M. R.; Pinlac, R. A. F.; Lesage, J.; Stern, C. L.; Poeppelmeier, K. R. *Z. Anorg. Allg. Chem.* **2009**, *635*, 869.
(14) Kong, F.; Huang, S.-P.; Sun, Z.-M.; Mao, J.-G.; Cheng, W.-D. *J. Am. Chem. Soc.* **2006**, *128*, 7750.
(15) Jiang, H.-L.; Huang, S.-P.; Fan, Y.; Mao, J.-G.; Cheng, W.-D. *Chem.—Eur. J.* **2008**, *14*, 1972.
(16) Mao, J.-G.; Jiang, H.-L.; Kong, F. *Inorg. Chem.* **2008**, *47*, 8498.
(17) Sun, C.-F.; Hu, C.-L.; Xu, X.; Ling, J.-B.; Hu, T.; Kong, F.; Long, X.-F.; Mao, J.-G. *J. Am. Chem. Soc.* **2009**, *131*, 9486.
(18) Li, P.-X.; Kong, F.; Hu, C.-L.; Zhao, N.; Mao, J.-G. *Inorg. Chem.* **2010**, *49*, 5943.
(19) Sun, C.-F.; Hu, C.-L.; Kong, F.; Yang, B.-P.; Mao, J.-G. *Dalton Trans.* **2010**, *39*, 1473.
(20) Zhang, S.-Y.; Hu, C.-L.; Sun, C.-F.; Mao, J.-G. *Inorg. Chem.* **2010**, *49*, 11627.
(21) Sun, C.-F.; Hu, C.-L.; Xu, X.; Yang, B.-P.; Mao, J.-G. *J. Am. Chem. Soc.* **2011**, *133*, 5561.
(22) Zhang, J.-H.; Hu, C.-L.; Xu, X.; Kong, F.; Mao, J.-G. *Inorg. Chem.* **2011**, *50*, 1973.
(23) Huang, Q.; Hwu, S.-J. *Inorg. Chem.* **2003**, *42*, 655.
(24) Mo, X.; Hwu, S.-J. *Inorg. Chem.* **2003**, *42*, 3978.
(25) Mo, X.; Ferguson, E.; Hwu, S.-J. *Inorg. Chem.* **2005**, *44*, 3121.
(26) Queen, W., L.; West, J. P.; Hwu, S.-J.; VanDerveer Donald, G.; Zarzyczny Matthew, C.; Pavlick Ryan, A. *Angew. Chem., Int. Ed.* **2008**, *47*, 3791.
(27) Gutnick, J. R.; Muller, E. A.; Sarjeant, A. N.; Norquist, A. J. *Inorg. Chem.* **2004**, *43*, 6528.
(28) Muller, E. A.; Cannon, R. J.; Sarjeant, A. N.; Ok, K. M.; Halasyamani, P. S.; Norquist, A. J. *Cryst. Growth Des.* **2005**, *5*, 1913.
(29) Veltman, T. R.; Stover, A. K.; Sarjeant, A. N.; Ok, K. M.; Halasyamani, P. S.; Norquist, A. J. *Inorg. Chem.* **2006**, *45*, 5529.
(30) Choyke, S. J.; Blau, S. M.; Larner, A. A.; Narducci, S. A.; Yeon, J.; Halasyamani, P. S.; Norquist, A. J. *Inorg. Chem.* **2009**, *48*, 11277.
(31) Bi, W.; Leblanc, N.; Mercier, N.; Senzier-Auban, P.; Pasquier, C. *Chem. Mater.* **2009**, *27*, 4099.
(32) Leblanc, N.; Mercier, N.; Zorina, L.; Simonov, S.; Auban-Senzier, P.; Pasquier, C. *J. Am. Chem. Soc.* **2011**, *133*, 14924.
(33) Bera, T. K.; Jang, J. I.; Song, J.-H.; Malliakas, C. D.; Freeman, A. J.; Ketterson, J. B.; Kanatzidis, M. G. *J. Am. Chem. Soc.* **2010**, *132*, 3484.
(34) Chung, I.; Jang, J.-I.; Malliakas, C. D.; Ketterson, J. B.; Kanatzidis, M. G. *J. Am. Chem. Soc.* **2010**, *132*, 384.
(35) Opik, U.; Pryce, M. H. L. *Proc. R. Soc. A* **1957**, *238*, 425.
(36) Bader, R. F. W. *Mol. Phys.* **1960**, *3*, 137.
(37) Bader, R. F. W. *Can. J. Chem.* **1962**, *40*, 2140.
(38) Pearson, R. G. *J. Am. Chem. Soc.* **1969**, *91*, 4947.
(39) Pearson, R. G. *THEOCHEM* **1983**, *12*, 25.
(40) Wheeler, R. A.; Whangbo, M. H.; Hughbanks, T.; Hoffmann, R.; Burdett, J. K.; Albright, T. A. *J. Am. Chem. Soc.* **1986**, *108*, 2222.
(41) Goodenough, J. B. *Annu. Rev. Mater. Sci.* **1998**, *28*, 1.
(42) Halasyamani, P. S.; Poeppelmeier, K. R. *Chem. Mater.* **1998**, *10*, 2753.
(43) Goodey, J.; Ok, K. M.; Broussard, J.; Hofmann, C.; Escobedo, F. V.; Halasyamani, P. S. *J. Solid State Chem.* **2003**, *175*, 3.
(44) Chi, E. O.; Gandini, A.; Ok, K. M.; Zhang, L.; Halasyamani, P. S. *Chem. Mater.* **2004**, *16*, 3616.
(45) Sivakumar, T.; Chang, H. Y.; Baek, J.; Halasyamani, P. S. *Chem. Mater.* **2007**, *19*, 4710.
(46) Chang, H. Y.; Sivakumar, T.; Ok, K. M.; Halasyamani, P. S. *Inorg. Chem.* **2008**, *47*, 8511.
(47) Chang, H. Y.; Kim, S.-H.; Ok, K. M.; Halasyamani, P. S. *Chem. Mater.* **2009**, *21*, 1654.
(48) Choi, M.-H.; Kim, S.-H.; Chang, H.-Y.; Halasyamani, P. S.; Ok, K. M. *Inorg. Chem.* **2009**, *48*, 8376.
(49) Chang, H. Y.; Kim, S. W.; Halasyamani, P. S. *Chem. Mater.* **2010**, *22*, 3241.
(50) Yang, T.; Sun, J.; Yeon, J.; Halasyamani, P. S.; Huang, S.; Hemberger, J.; Greenblatt, M. *Chem. Mater.* **2010**, *22*, 4814.
(51) Nguyen, S. D.; Kim, S.-H.; Halasyamani, P. S. *Inorg. Chem.* **2011**, *50*, 5215.
(52) Halasyamani, P. S.; O'Hare, D. *Inorg. Chem.* **1997**, *36*, 6409.
(53) Millet, P.; Galy, J.; Johnsson, M. *Solid State Sci.* **1999**, *1*, 279.
(54) Dai, Z.; Shi, Z.; Li, G.; Chen, X.; Lu, X.; Xu, Y.; Feng, S. *J. Solid State Chem.* **2003**, *172*, 205.
(55) Kim, Y.-T.; Kim, Y.-H.; Park, K.; Kwon, Y.-U.; Young, V. G. Jr. *J. Solid State Chem.* **2001**, *161*, 23.
(56) Lee, K.-S.; Kwon, Y.-U.; Namgung, H.; Kim, S.-H. *Inorg. Chem.* **1995**, *34*, 4178.
(57) Kwon, Y.-U.; Lee, K.-S.; Kim, Y. H. *Inorg. Chem.* **1996**, *35*, 1161.
(58) Pitzschke, D.; Jansen, M. *Z. Anorg. Allg. Chem.* **2007**, *633*, 1563.
(59) Harrison, W. T. A.; Dussack, L. L.; Jacobson, A. J. *Acta Crystallogr., Sect. C: Cryst. Struct. Commun.* **1995**, *C51*, 2473.
(60) Sivakumar, T.; Ok, K. M.; Halasyamani, P. S. *Inorg. Chem.* **2006**, *45*, 3602.
(61) *SAINT, Program for Area Detector Absorption Correction*, 4.05; Siemens Analytical X-ray Systems: Madison, WI, 1995.
(62) Sheldrick, G. M. *SHELXS-97, A program for Automatic Solution of Crystal Structures*; University of Göttingen: Göttingen, Germany, 1997.
(63) Sheldrick, G. M. *SHELXL-97, A program for Crystal Structure Refinement*; University of Göttingen: Göttingen, Germany, 1997.
(64) Farrugia, L. J. *J. Appl. Crystallogr.* **1999**, *32*, 837.
(65) Kubelka, P.; Munk, F. *Z. Tech. Phys.* **1931**, *12*, 593.
(66) Ok, K. M.; Chi, E. O.; Halasyamani, P. S. *Chem. Soc. Rev.* **2006**, *35*, 710.
(67) Kurtz, S. K.; Perry, T. T. *J. Appl. Phys.* **1968**, *39*, 3798.
(68) Momma, K.; Izumi, F. *J. Appl. Crystallogr.* **2008**, *41*, 653.
(69) Brown, I. D.; Altermatt, D. *Acta Crystallogr., Sect. B* **1985**, *B41*, 244.
(70) Brown, I. D. *The Chemical Bond in Inorganic Chemistry*; Oxford University Press: New York, 2002; Vol. *12*.
(71) Hou, J. Y.; Huang, C. C.; Zhang, H. H.; Yang, Q. Y.; Chen, Y. P.; Xu, J. F. *Acta Crystallogr., Sect. C: Cryst. Struct. Commun.* **2005**, *C61*, i59.

(72) Giester, G. *Monatsh. Chem.* **1993**, *124*, 1107.
(73) Lafront, A.-M.; Bonvoisin, J.; Trombe, J.-C. *J. Solid State Chem.* **1996**, *122*, 130.
(74) Ok, K. M.; Halasyamani, P. S. *Chem. Mater.* **2002**, *14*, 2360.
(75) Rider, E. E.; Sarin, V. A.; Bydanov, N. N.; Vinogradova, I. S. *Kristallografiya* **1985**, *30*, 1007.
(76) Makarova, I. P.; Muradyan, L. A.; Rider, E. E.; Sarin, V. A.; Vinogradova, I. S.; Simonov, V. I. *Kristallografiya* **1990**, *35*, 889.
(77) Delage, C.; Carpy, A.; Goursolle, M. *Acta Crystallogr., Sect. B* **1982**, *B38*, 1278.
(78) Effenberger, H. *Acta Crystallogr., Sect. C: Cryst. Struct. Commun.* **1987**, *C43*, 182.
(79) Koskenlinna, M.; Valkonen, J. *Acta Crystallogr., Sect. C: Cryst. Struct. Commun.* **1995**, *C51*, 1.
(80) Mueller, H.; Unterderweide, K.; Engelen, B. *Z. Kristallogr.* **1996**, *211*, 700.
(81) Giester, G.; Lengauer, C. L. *Monatsh. Chem.* **1998**, *129*, 445.
(82) Debye, P. *Phys. Z.* **1921**, *22*, 302.
(83) Debye, P. *Polar Molecules*; Chemical Catalog Company, Inc.: New York, NY, 1929.
(84) Zabrodsky, H.; Peleg, S.; Avnir, D. *J. Am. Chem. Soc.* **1992**, *114*, 7843.
(85) Alvarez, S.; Avnir, D.; Llunell, M.; Pinsky, M. *New J. Chem.* **2002**, *26*, 996.
(86) Alvarez, S.; Alemany, P.; Casanova, D.; Cirera, J.; Llunell, M.; Avnir, D. *Coord. Chem. Rev.* **2005**, *249*, 1693.
(87) Llunell, M.; Casanova, D.; Cirera, J.; Bofill, J. M.; Alemany, P.; Alvarez, S.; Pinsky, M.; Avnir, D. *SHAPE, 1.1b ed.*; University of Barcelona: Barcelona, Spain, 2004.
(88) Halasyamani, P. S. *Chem. Mater.* **2004**, *16*, 3586.
(89) Preiser, C.; Losel, J.; Brown, I. D.; Kunz, M.; Skowron, A. *Acta Crystallogr., Sect. B: Struct. Sci.* **1999**, *B55*, 698.
(90) Salinas-Sanchez, A.; Garcia-Munoz, J. L.; Rodriguez-Carvajal, J.; Saez-Puche, R.; Martinez, J. L. *J. Solid State Chem.* **1992**, *100*, 201.
(91) Trunov, V. K.; Velikodnyi, Y. A.; Murashova, E. V.; Zhuravlev, V. D. *Dokl. Akad. Nauk SSSR* **1983**, *270*, 886.
(92) Vedernikov, A. A.; Velikodnyi, Y. A.; Ilyukhin, V. V.; Trunov, V. K. *Dokl. Akad. Nauk SSSR* **1982**, *263*, 101.
(93) Yao, T.; Oka, Y.; Yamamoto, N. *Inorg. Chim. Acta* **1995**, *238*, 165.
(94) Gatehouse, B. M.; Guddat, L. W.; Roth, R. S. *J. Solid State Chem.* **1987**, *71*, 390.
(95) Parhi, P.; Manivannan, V.; Kohli, S.; McCurdy, P. *Bull. Mater. Sci.* **2008**, *31*, 885.
(96) Schnuriger, B.; Enjalbert, R.; Savariault, J. M.; Galy, J. *J. Solid State Chem.* **1991**, *95*, 397.
(97) Krivovichev, S. V.; Burns, P. C. *Can. Mineral.* **2003**, *41*, 951.
(98) Kim, S.-H.; Yeon, J.; Halasyamani, P. S. *Chem. Mater.* **2009**, *21*, 5335.
(99) Cohen, R. E. *Nature* **1992**, *358*, 136.